4D Automotive Radar Exploiting Sparse Array Optimization and Compressive Sensing

Ruxin Zheng[†], Shunqiao Sun[†], Wesley Kuo[‡], Theagenis Abatzoglou[‡], and Matt Markel[‡]

[†]Department of Electrical and Computer Engineering, The University of Alabama, Tuscaloosa, AL 35487
[‡]Spartan Radar, Los Alamitos, CA 90720

2023 57th Asilomar Conference on Signals, Systems, and Computers | 979-8-3503-2574-4/23/$31.00 ©2023 IEEE | DOI: 10.1109/IEEECONF59524.2023.10476872

***Abstract*—Automotive radar systems require high resolution in four dimensions: range, Doppler, elevation and azimuth. The angular resolution of an automotive radar are determined by the antenna array aperture. Two-dimensional (2D) antenna arrays are necessary for angle estimation in both elevation and azimuth for automotive radar systems to enable drive-over and drive-under functions. Sparse arrays offer advantages such as reduced mutual coupling and lower hardware costs. The sparse array configurations like coprime and nested arrays, which require a large number of array snapshots, may not be suitable for highly dynamic automotive scenarios. Multiple-input and multiple-output (MIMO) radars are widely adopted in automotive radar applications due to their ability to synthesize a large virtual array. In this paper, our objective is to optimize the geometry of 2D MIMO sparse arrays while considering fabrication constraints, i.e., minimal spacing between antennas. This optimization aims to minimize the peak sidelobe level and half-power beam width (HPBW), thus enabling high-resolution imaging with single snapshot. Angle finding is accomplished through a 2D compressive sensing approach. Through extensive numerical experiments, we demonstrate that the proposed workflow offers a practical solution for 2D MIMO sparse arrays, ensuring high angular resolution in automotive radar systems.**

***Index Terms*—Automotive radar, Constrained optimization, Sparse array optimization**

I. Introduction

Radar technology has emerged as a crucial component in autonomous driving systems, primarily due to its robustness in adverse weather conditions [1, 2]. For an automotive radar system to meet the demands of autonomous driving, it must provide high-resolution information in four dimensions (4D), encompassing range, Doppler, azimuth and elevation angles, while maintaining cost-effectiveness for mass production [3]. The range and Doppler resolution of an automotive radar are determined by the bandwidth of the radar waveform and the coherent processing interval (CPI), respectively. State-of-the-art automotive frequency-modulated continuous wave (FMCW) radar systems typically operate within the frequency band of 76-81 GHz. This frequency range allows for the use of relatively compact antennas that can be discreetly installed behind the vehicle's bumper. Additionally, the broad available bandwidth enables high-resolution target-range measurements.

The range and Doppler parameters of targets can be estimated using a single receive antenna. However, to estimate the angle parameters of targets, a receive antenna array is needed. The angular resolution depends on the antenna array's aperture size. To achieve high-resolution 4D radar imaging for autonomous driving applications, automotive radars need to occupy a substantial bandwidth, employ a sufficiently long CPI, and feature a sizable antenna aperture in both horizontal and vertical directions. However, meeting these requirements presents significant challenges, particularly when using a filled array approach, which often requires a high number of antennas to achieve the desired aperture. To address this issue, sparse arrays have gained attention as an effective and economical solution for automotive radar systems [3–6]. Sparse arrays achieve a larger aperture and improved angular resolution with the same number of elements, making them a promising alternative to filled arrays. Furthermore, the large element spacing in sparse arrays can also reduce mutual coupling [7].

An overview of the two-dimensional (2D) sparse arrays and corresponding direction of arrival (DOA) estimation algorithms was given in [8]. The 2D sparse planar arrays generally fall into two categories. The first category involves additional DOA estimation steps, such as coprime planar arrays (CPA) [9] or general coprime planar arrays (GCPA) [10] which interleave two uniform planar arrays with coprime inter-element spacing. Target pairing and dealiasing between ambiguous peaks observed within each subarray are necessary to provide the final DOA estimation. These steps can significantly increase the computational burden. The second category embraces the concept of the difference coarray, exemplified by nested planar arrays (NPA) [11, 12], which synthesize a virtual array by considering the cross correlation between two physical sensors in the array. However, the effective application of difference coarrays relies on precise covariance matrix estimation, which, in turn, requires multiple snapshots and the sources to be non-coherent. Consequently, these 2D sparse planar arrays may not be suitable for automotive radars, which often operate in highly dynamic scenarios with limited snapshots.

Alternatively, 2D sparse array geometries for automotive radar systems can be optimized such that the peak sidelobe level (PSL) is minimized, while maintaining a narrow half power beam width (HPBW). Rather than relying on exhaustive search methods, researchers have explored various approaches in the literature to derive these desired sparse array geometries. These approaches often utilize heuristic algorithms such as genetic algorithms (GA) [13], simulated annealing (SA) [14], and particle swarm optimization (PSO) [15], with a primary focus on reducing PSL and achieving a narrow HPBW. It should be noted that automotive radar can have different coverage in range and field of view (FOV). For instance, short-range radars (SRR) with an azimuth FOV of $[-75^\circ, 75^\circ]$ and a detection range of 45 meters are commonly positioned at the vehicle's corners for tasks like blind-spot detection and cross-traffic alerts. Mid-range radars (MRR), with an azimuth FOV of $[-40^\circ, 40^\circ]$ and a detection range of 100 meters, are installed on the vehicle's front and rear sides to assist in lane-change maneuvers and automatic emergency braking. Long-range radars (LRR) with an azimuth FOV of $[-15^\circ, 15^\circ]$ and a detection range of 250 meters are typically placed at the vehicle's front to support adaptive cruise control. Thus, when optimizing array geometry, the focus should be on minimizing PSL within the specific FOV, while high PSL or even grating lobes outside the FOV can be addressed through antenna element design [1].

High-resolution direction-of-arrival (DOA) estimation algorithms are desired to achieve high angular resolution for automotive radar to enable environmental perception for autonomous vehicles [16]. Subspace-based high-resolution DOA estimation methods, such as

MUSIC [17–19], ESPRIT [20–22], matrix pencil methods [23, 24], requires multiple snapshots to estimate the signal and noise subspace. High-resolution DOA estimation algorithms that work under a single snapshot, such as compressive sensing [25], are highly desired for automotive radars. The compressive sensing algorithm demands that the dictionary matrix adheres to the restricted isometry property (RIP), or low mutual coherence for the dictionary matrix.

In the realm of automotive radar applications, multiple-input and multiple-output (MIMO) radar [26, 27] has gained increasing popularity due to its cost-efficient ability to synthesize large virtual arrays, thereby providing high angular resolution with low hardware cost [1]. Moreover, the missing antenna information from a sparse MIMO radar signal can be estimated using a 2D variant of the missing-data iterative adaptive approach (MIAA) and subsequently detecting objects and their locations within the radar array's field of view through multi-dimensional folding (MDF) [28].

In this paper, we introduce a novel workflow for designing 2D MIMO sparse arrays tailored for automotive radar applications. Our approach begins with formulating sparse array optimization as a constrained optimization problem, with a primary objective of minimizing the PSL and the beam width of the main lobe within a defined FOV. Additionally, we account for real-world fabrication constraints, such as the minimum required distance between antennas, ensuring the practical manufacturability of our optimized array geometry. Furthermore, we propose the incorporation of a 2D sparse super-resolution algorithm, such as compressive sensing [25], which effectively enhances angular resolution even when a limited number of array snapshots are available, thereby further improving the angle finding performance. Our contribution lies in offering a practical solution for 2D MIMO sparse array design within automotive radar systems, enabling high angular resolution with a restricted number of snapshots and antennas.

II. System Model

In this section, we introduce the signal model of the 2D MIMO array, followed by the definition of the concept of the 2D array response, PSL, and HPBW. Additionally, we describe the physical constraints associated with the antenna elements.

A. Signal Model

Consider a planar array of a MIMO radar system situated on the x-y plane with M_t transmitting antennas and M_r receiving antennas. The x- and y-coordinates of transmitting antenna and receiving antennas are defined as:

$$\mathbf{x}_t = \begin{bmatrix} x_{t1} \\ x_{t2} \\ \vdots \\ x_{tM_t} \end{bmatrix}, \mathbf{y}_t = \begin{bmatrix} y_{t1} \\ y_{t2} \\ \vdots \\ y_{tM_t} \end{bmatrix}, \mathbf{x}_r = \begin{bmatrix} x_{r1} \\ x_{r2} \\ \vdots \\ x_{rM_r} \end{bmatrix}, \mathbf{y}_r = \begin{bmatrix} y_{r1} \\ y_{r2} \\ \vdots \\ y_{rM_r} \end{bmatrix}. \tag{1}$$

A virtual array of size $M_t \times M_r$ can be synthesized using M_t transmitting antennas and M_r receiving antennas. The x- and y-coordinates of these virtual antennas corresponding to the n-th transmitting antenna can be expressed as follows:

$$\begin{aligned} \mathbf{x}_{vn} &= \left[x_{tn} + x_{r1}, x_{tn} + x_{r2}, \cdots, x_{tn} + x_{rM_r}\right]^T, \\ \mathbf{y}_{vn} &= \left[y_{tn} + y_{r1}, y_{tn} + y_{r2}, \cdots, y_{tn} + y_{rM_r}\right]^T. \end{aligned} \tag{2}$$

Then, the x- and y-coordinates of virtual arrays corresponding to all transmitting antennas can be expressed as $\mathbf{x}_v = [\mathbf{x}_{v1}^T, \mathbf{x}_{v2}^T, \cdots, \mathbf{x}_{vM_t}^T]^T$ and $\mathbf{y}_v = [\mathbf{y}_{v1}^T, \mathbf{y}_{v2}^T, \cdots, \mathbf{y}_{vM_t}^T]^T$, respectively. Furthermore, we define the MIMO process as $[\mathbf{x}_v, \mathbf{y}_v] = \mathbf{MIMO}(\mathbf{x}_t, \mathbf{y}_t, \mathbf{x}_r, \mathbf{y}_r)$. Fig. 1 shows a MIMO radar with 3 transmit antennas and 4 receive antennas that are obtained from a single automotive radar transceiver, and the transmit and receive antennas are randomly deployed in an area of $[0, 11](\lambda/2) \times [0, 11](\lambda/2)$ to synthesize a MIMO 2D virtual sparse array of 12 elements. Subsequently, we can express the steering vectors associated with the synthesized virtual array as follows:

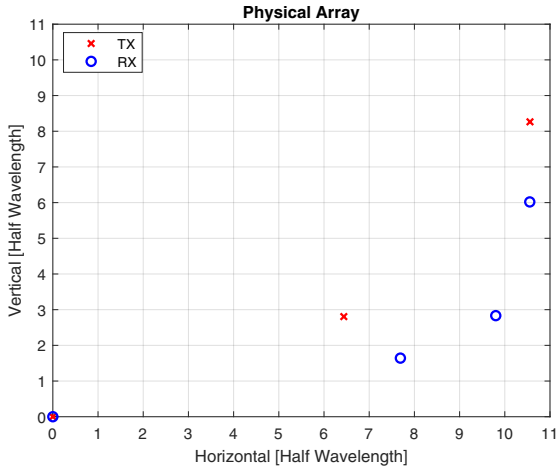

(a)

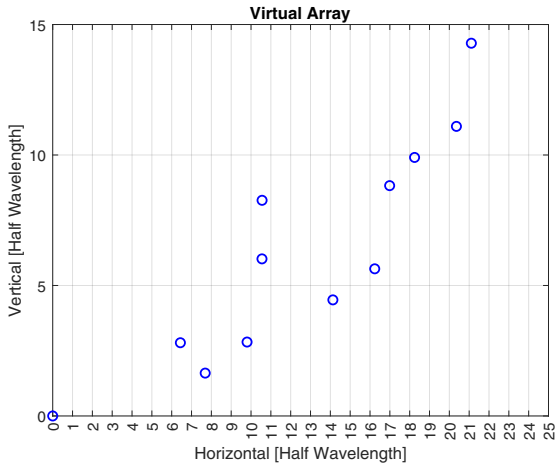

(b)

Fig. 1: A MIMO radar with 3 transmit antennas and 4 receive antennas. The transmit and receive antennas are randomly deployed in an area of $[0, 11](\lambda/2) \times [0, 11](\lambda/2)$ to synthesize a MIMO 2D virtual array of 12 elements. The reference position is fixed at the origin for both the first transmit and receive antennas.

$$\mathbf{a}(\psi_x, \psi_y) = \exp(j\frac{2\pi}{\lambda}(\mathbf{x}_v\psi_x + \mathbf{y}_v\psi_y)), \tag{3}$$

where,

$$\begin{aligned} \psi_x &= sin(\theta)cos(\phi), \\ \psi_y &= sin(\theta)sin(\phi). \end{aligned} \tag{4}$$

Here, θ and ϕ denote the azimuth and elevation angle, respectively.

B. 2D Ambiguity Function

The characteristics of array geometry can be effectively described using the ambiguity function (AF). In this context, we define the 2D AF as:

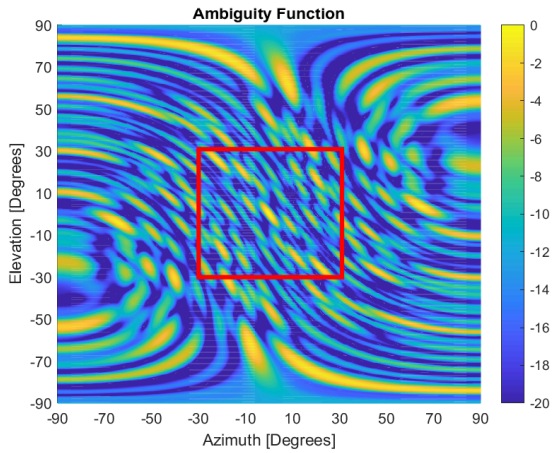

Fig. 2: The AF of the randomly generated sparse array shown in Fig. 1, with the region inside the red box representing the FOV of interest.

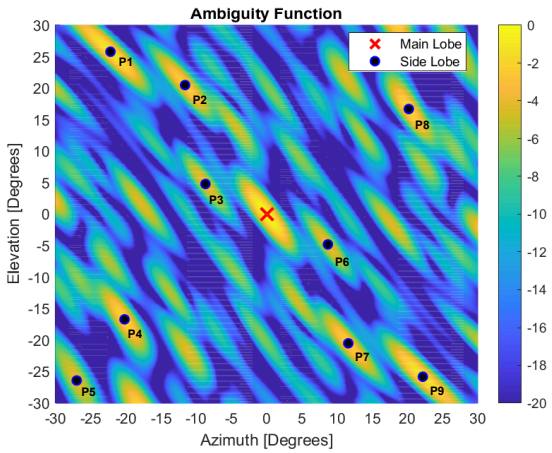

Fig. 3: The zoomed-in AF of the randomly generated sparse array, where the red cross denotes the main lobe, while the black dots represent the side lobes. For simplicity, we only show markers for 9 side lobes.

$$AF(\theta,\phi,\theta_t,\phi_t) = \left|\mathbf{a}(\theta,\phi)^H \mathbf{a}(\theta_t,\phi_t)\right| = \left|\sum_{n=1}^{M_t M_r} a_n(\theta-\theta_t,\phi-\phi_t)\right|. \quad (5)$$

In this equation, θ and ϕ denote the scan azimuth and elevation angles, respectively, while θ_t and ϕ_t correspond to the target's azimuth and elevation angles. It's important to note that the AF primarily relates to the array geometry rather than the target's angles. For simplicity, we set $\theta_t = 0^\circ$ and $\phi_t = 0^\circ$. The AF of the virtual array depicted in Fig. 1 with $[-30^\circ, 30^\circ]$ FOV in both azimuth and elevation is illustrated in Fig. 2.

C. PSL & HPBW

In this paper, we aim to design the 2D MIMO sparse arrays such that the PSL and HPBW within narrow down FOV are optimized. In Fig. 3, we present a zoomed-in view of the AF for the randomly generated sparse array. The red cross represents the main lobe, while the black dots denote the side lobes. Therefore, the PSL of the AF is defined as

$$f_{\mathrm{PSL}}(x_t,y_t,x_r,y_r) = \max\{P_1,P_2,\cdots,P_n\}, \quad (6)$$

where P_n represents the magnitude of the n-th side lobe.

In Fig. 4, we plot the the zoomed-in main lobe, and the -3 dB magnitude contour whose magnitude is half of the main lobe peak value, equivalent to a decrease of -3 dB in normalized magnitude. We sample n points along the -3 dB magnitude contour in all directions to ensure uniform resolution. The main lobe HPBW is defined as

$$f_{\mathrm{HPBW}}(x_t,y_t,x_r,y_r) = \max\{d_1,d_2,\cdots,d_n\}, \quad (7)$$

where d_n is the distance between the n-th sampling point, S_n, and the location of the main lobe peak.

D. Physical Constraints

The optimized array geometry should exhibit low PSL and a narrow HPBW while remaining feasible for real-world fabrication, considering the physical size of radar antennas. Notably, mutual coupling is inversely proportional to the spacing between antenna elements and decreases significantly when the inter-element spacing

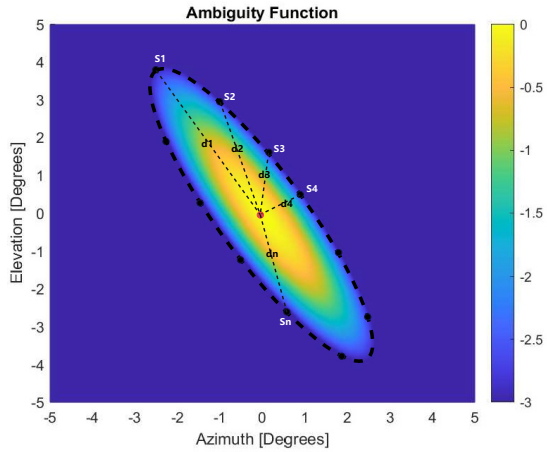

Fig. 4: The zoomed-in main lobe in the AF of the randomly generated sparse array.

exceeds half a wavelength, thereby reducing the burden of array calibration [29]. Additionally, we must define the maximum array aperture in both the x- and y-coordinates.

The physical constraints on the x- and y-coordinates of the transmitting antennas are defined as follows:

$$\begin{aligned} \max\{x_{t1},x_{t2},\cdots,x_{tM_t}\} &\le \mathbf{X}_{tmax}, \\ |x_{ti}-x_{t(i-1)}| &\ge \Delta\mathbf{X}_t, \qquad i=1,\cdots,M_t, \\ \max\{y_{t1},y_{t2},\cdots,y_{tM_t}\} &\le \mathbf{Y}_{tmax}, \\ |y_{ti}-y_{t(i-1)}| &\ge \Delta\mathbf{Y}_t, \qquad i=1,\cdots,M_t. \end{aligned} \quad (8)$$

Here, $\mathbf{X}_{tmax}$ is the maximum allowable x-coordinate, and $\mathbf{Y}_{tmax}$ is the maximum allowable y-coordinate. $\Delta\mathbf{X}_t$ is the minimum allowed spacing between two antenna elements along the x-direction, and $\Delta\mathbf{Y}_t$ is the minimum allowed spacing between two transmitting antenna elements along the y-direction.

The physical constraints on the x- and y-coordinates of the receiving antennas are defined as follows:

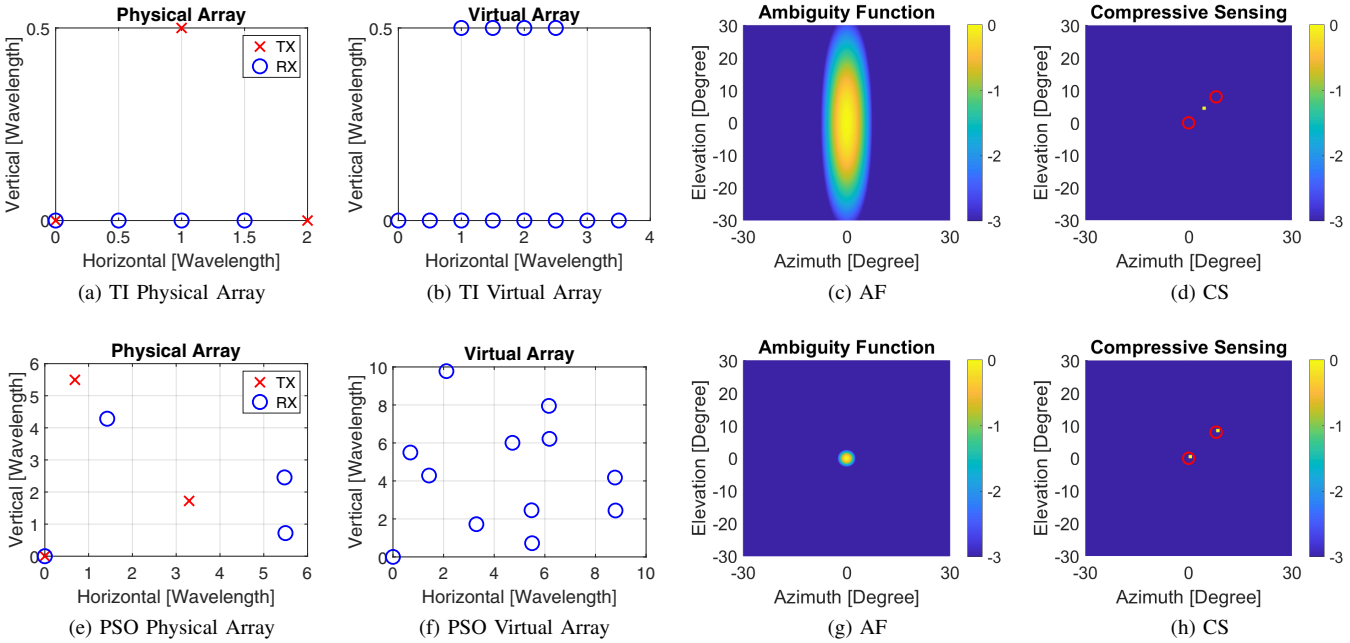

(a) TI Physical Array (b) TI Virtual Array (c) AF (d) CS

(e) PSO Physical Array (f) PSO Virtual Array (g) AF (h) CS

Fig. 5: The performance evaluation of TI AWR2243 and optimized Array via PSO. TI AWR2243: (a) physical array, (b) virtual array, (c) AF, (d) CS detection results; The optimized array via PSO: (e) physical array, (f) virtual array, (g) AF, (h) CS detection results.

$$\begin{aligned} \max\{x_{r1}, x_{r2}, \cdots, x_{rM_r}\} &\leq \mathbf{X}_{rmax}, \\ |x_{ri} - x_{r(i-1)}| &\geq \Delta\mathbf{X}_r, \qquad i = 1, \cdots, M_r, \\ \max\{y_{r1}, y_{r2}, \cdots, y_{rM_r}\} &\leq \mathbf{Y}_{rmax}, \\ |y_{ri} - y_{r(i-1)}| &\geq \Delta\mathbf{Y}_r, \qquad i = 1, \cdots, M_r. \end{aligned} \tag{9}$$

Here, $\mathbf{X}_{rmax}$ is the maximum allowable x-coordinate, and $\mathbf{Y}_{rmax}$ is the maximum allowable y-coordinate. $\Delta\mathbf{X}_r$ is the minimum allowed spacing between two antenna elements along the x-direction, and $\Delta\mathbf{Y}_r$ is the minimum allowed spacing between two receiving antenna elements along the y-direction.

III. Optimization Problem Formulation

When working with a limited number of antenna elements, a trade-off inevitably arises between achieving a lower PSL and a narrower HPBW. To strike this balance effectively, we establish a PSL threshold. In essence, our objective becomes optimizing the antenna geometry in a way that allows us to attain the narrowest possible HPBW while ensuring that the PSL remains below the defined threshold. Hence, the PSL with a specified threshold, ϵ, is defined as follows:

$$f_{\text{PSL}}(x_t, y_t, x_r, y_r, \epsilon) = \begin{cases} \text{PSL} & \text{if PSL} \geq \epsilon, \\ \epsilon & \text{Otherwise.} \end{cases} \tag{10}$$

The cost function $J(x_t, y_t, x_r, y_r, \epsilon)$ is defined as the summation of PSL and HPBW with weighting coefficient $0 < \alpha < 1$.

$$\begin{aligned} J(x_t, y_t, x_r, y_r, \epsilon) =& \alpha f_{\text{PSL}}(x_t, y_t, x_r, y_r, \epsilon) \\ &+ (1-\alpha) f_{\text{HPBW}}(x_t, y_t, x_r, y_r). \end{aligned} \tag{11}$$

Combining the cost function and the aforementioned antenna physical constraints, the 2D MIMO sparse array geometry optimization problem can be formulated as follows:

$$\begin{aligned} \min_{x_t, y_t, x_r, y_r} \quad & J(x_t, y_t, x_r, y_r, \epsilon) \\ \text{s.t.} \quad & \epsilon < 0 \\ & \max\{x_{t1}, x_{t2}, \cdots, x_{tM_t}\} \leq \mathbf{X}_{tmax}, \\ & |x_{ti} - x_{t(i-1)}| \geq \Delta\mathbf{X}_t, \qquad i = 1, \cdots, M_t, \\ & \max\{y_{t1}, y_{t2}, \cdots, y_{tM_t}\} \leq \mathbf{Y}_{tmax}, \\ & |y_{ti} - y_{t(i-1)}| \geq \Delta\mathbf{Y}_t, \qquad i = 1, \cdots, M_t, \\ & \max\{x_{r1}, x_{r2}, \cdots, x_{rM_r}\} \leq \mathbf{X}_{rmax}, \\ & |x_{ri} - x_{r(i-1)}| \geq \Delta\mathbf{X}_r, \qquad i = 1, \cdots, M_r, \\ & \max\{y_{r1}, y_{r2}, \cdots, y_{rM_r}\} \leq \mathbf{Y}_{rmax}, \\ & |y_{ri} - y_{r(i-1)}| \geq \Delta\mathbf{Y}_r, \qquad i = 1, \cdots, M_r. \end{aligned} \tag{12}$$

The constrained optimization problem can be addressed through heuristic algorithms like GA, SA, and PSO. In this study, we have opted for PSO to perform this optimization.

IV. Performance Evaluation

The Texas Instruments (TI) AWR2243 is a single-chip 76-81 GHz FMCW transceiver with 3 transmitting antennas and 4 receiving antennas. Each TX/RX antenna element is implemented as a series-fed microstrip patch array. The wavelength, λ, in free space at 78.5 GHz corresponds to 3.8 mm, and the antenna size measures approximately $1.4\text{mm} \times 10\text{mm}$. In alignment with the TI AWR2243 configuration, we set $M_t = 3$ for the transmitting antennas and $M_r = 4$ for the receiving antennas. The minimum allowed interelement spacing along both the x and y directions is specified as $\Delta\mathbf{X}_t = \Delta\mathbf{X}_r = 0.5\lambda$ and $\Delta\mathbf{Y}_t = \Delta\mathbf{Y}_r = 3\lambda$. Assuming the deployment of Tx and Rx antennas within an area of $[0, 11](\lambda/2) \times [0, 11](\lambda/2)$, we define $\mathbf{X}_{tmax} = \mathbf{X}_{rmax} = 5.5\lambda$ and $\mathbf{Y}_{tmax} = \mathbf{Y}_{rmax} = 5.5\lambda$.

Furthermore, we establish the reference point at the origin for both transmitting and receiving antennas. We set $\epsilon = -6$ dB, and define the specific FOV for both azimuth and elevation as $[-30^\circ, 30^\circ]$. Thus, the optimization variables are continuous and are represented as:

$$\mathbf{x}_t = \begin{bmatrix} 0 \\ x_{t2} \\ x_{t3} \end{bmatrix}, \mathbf{y}_t = \begin{bmatrix} 0 \\ y_{t2} \\ y_{t3} \end{bmatrix}, \mathbf{x}_r = \begin{bmatrix} 0 \\ x_{r2} \\ x_{r3} \\ x_{r4} \end{bmatrix}, \mathbf{y}_r = \begin{bmatrix} 0 \\ y_{r2} \\ y_{r3} \\ y_{r4} \end{bmatrix}. \quad (13)$$

The physical and virtual arrays of the TI AWR2243 are depicted in Fig. 5(a) and Fig. 5(b), respectively. As illustrated, the synthesized virtual array exhibits a horizontal aperture of 3.5λ and a vertical aperture of 0.5λ. Due to this small aperture size, the AF of the TI AWR2243, shown in Fig. 5(c), possesses a wide azimuth HPBW and an even wider elevation HPBW. Consequently, it exhibits relatively low angular resolution. Assume there are two targets, one at $[0^\circ, 0^\circ]$ and another at $[8^\circ, 8^\circ]$, both with a 40 dB signal-to-noise ratio (SNR). As seen in Fig. 5(d), the TI AWR2243 struggles to detect both targets using 2D compressive sensing (CS). In contrast, the physical and virtual arrays of the PSO-optimized array geometry are presented in Fig. 5(e) and Fig. 5(f), respectively. The optimized array boasts a horizontal aperture of 9λ and a vertical aperture of 10λ. As shown in Fig. 5(g), the AF of the optimized array features a much narrower HPBW in all directions, leading to significantly improved angular resolution. Consequently, as depicted in Fig. 5(h), the optimized array successfully resolves both targets using 2D CS.

V. Conclusion

In this paper, we has proposed an innovative approach to design 2D array geometry for 4D automotive radar systems. Instead of carrying out exhaustive search to determine the desired array layout, we formulated the array geometry design challenge as a constrained optimization problem. We aim to minimize both the PSL within a specific narrow FOV and the beam width of the main lobe in the sparse arrays ambiguity function, by considering the fabrication constraints to ensure that the optimized solution is feasible for implementation. The PSO heuristic algorithm has been applied to tackle this constrained optimization problem. To benchmark our approach, we utilize the TI AWR2243 as the baseline geometry. Upon comparing our optimized array geometry with the TI AWR2243, we demonstrate that the optimized sparse array configuration provides superior angular resolution with the same number of antenna elements.

References

[1] S. Sun, A. P. Petropulu, and H. V. Poor, "MIMO radar for advanced driver-assistance systems and autonomous driving: Advantages and challenges," *IEEE Signal Processing Magazine*, vol. 37, no. 4, pp. 98–117, 2020.

[2] M. Markel, *Radar for Fully Autonomous Driving*. Boston, MA: Artech House, 2022.

[3] S. Sun and Y. D. Zhang, "4D automotive radar sensing for autonomous vehicles: A sparsity-oriented approach," *IEEE J. Sel. Topics Signal Process.*, vol. 15, no. 4, pp. 879–891, 2021.

[4] S. Sun and A. P. Petropulu, "A sparse linear array approach in automotive radars using matrix completion," in *Proc. IEEE 45th Int. Conf. on Acoustics, Speech, and Signal Processing (ICASSP)*, Barcelona, Spain, May 4-8, 2020.

[5] S. Sun and Y. D. Zhang, "Four-dimensional high-resolution automotive radar imaging exploiting joint sparse-frequency and sparse-array design," in *IEEE International Conference on Acoustics, Speech, and Signal Processing (ICASSP)*, 2021, pp. 8413–8417.

[6] L. Xu, S. Sun, K. V. Mishra, and Y. D. Zhang, "Automotive FMCW radar with difference co-chirps," *IEEE Transactions on Aerospace and Electronic Systems*, in press, 2023.

[7] B. Friedlander and A. J. Weiss, "Direction finding in the presence of mutual coupling," *IEEE Transactions on Antennas and Propagation*, vol. 39, no. 3, pp. 273–284, 1991.

[8] I. Aboumahmoud, A. Muqaibel, M. Alhassoun, and S. Alawsh, "A review of sparse sensor arrays for two-dimensional direction-of-arrival estimation," *IEEE Access*, vol. 9, pp. 92 999–93 017, 2021.

[9] Q. Wu, F. Sun, P. Lan, G. Ding, and X. Zhang, "Two-dimensional direction-of-arrival estimation for co-prime planar arrays: A partial spectral search approach," *IEEE Sensors Journal*, vol. 16, no. 14, pp. 5660–5670, 2016.

[10] W. Zheng, X. Zhang, and H. Zhai, "Generalized coprime planar array geometry for 2-d doa estimation," *IEEE Communications Letters*, vol. 21, no. 5, pp. 1075–1078, 2017.

[11] P. Pal and P. Vaidyanathan, "Nested arrays in two dimensions, part I: Geometrical considerations," *IEEE Transactions on Signal Processing*, vol. 60, no. 9, pp. 4694–4705, 2012.

[12] ——, "Nested arrays in two dimensions, part II: Application in two dimensional array processing," *IEEE Transactions on Signal Processing*, vol. 60, no. 9, pp. 4706–4718, 2012.

[13] K. Chen, X. Yun, Z. He, and C. Han, "Synthesis of sparse planar arrays using modified real genetic algorithm," *IEEE Transactions on Antennas and Propagation*, vol. 55, no. 4, pp. 1067–1073, 2007.

[14] T. Pavlenko, C. Reustle, Y. Dobrev, M. Gottinger, L. Jassoume, and M. Vossiek, "Design and optimization of sparse planar antenna arrays for wireless 3-D local positioning systems," *IEEE Transactions on Antennas and Propagation*, vol. 65, no. 12, pp. 7288–7297, 2017.

[15] X. He, C. Alistarh, and S. K. Podilchak, "Optimal MIMO sparse array design based on simulated annealing particle swarm optimization," in *2022 16th European Conference on Antennas and Propagation (EuCAP)*. IEEE, 2022, pp. 1–5.

[16] R. Zheng, S. Sun, H. Liu, and T. Wu, "Deep neural networks-enabled vehicle detection using high-resolution automotive radar imaging," *IEEE Transactions on Aerospace and Electronic Systems*, vol. 59, no. 5, pp. 4815–4830, 2023.

[17] T. J. Abatzoglou, J. M. Mendel, and G. A. Harada, "The constrained total least squares technique and its applications to harmonic superresolution," *IEEE Transactions on Signal Processing*, vol. 39, no. 5, pp. 1070–1087, 1991.

[18] A. L. Swindlehurst and T. Kailath, "A performance analysis of subspace-based methods in the presence of model errors: Part I - the MUSIC algorithm," *IEEE Transactions on Signal Processing*, vol. 40, no. 7, pp. 1758–1774, 1992.

[19] ——, "A performance analysis of subspace-based methods in the presence of model errors: Part II - multidimensional algorithms," *IEEE Transactions on Signal Processing*, vol. 41, no. 9, pp. 2882–2890, 1993.

[20] A. L. Swindlehurst, B. Ottersten, R. Roy, and T. Kailath, "Multiple invariance ESPRIT," *IEEE Transactions on Signal Processing*, vol. 40, no. 4, pp. 867–881, 1992.

[21] M. Haardt and J. Nossek, "Unitary ESPRIT: How to obtain increased estimation accuracy with a reduced computational burden," *IEEE Trans. Signal Process.*, vol. 43, no. 5, pp. 1232–1242, 1995.

[22] M. D. Zoltowski, M. Haardt, and C. Mathews, "Closed-form 2-D angle estimation with rectangular arrays in element space or beamspace via unitary ESPRIT," *IEEE Trans. Signal Process.*, vol. 44, no. 2, pp. 316–328, 1996.

[23] Y. Hua and T. K. Sarkar, "Matrix pencil method for estimating parameters of exponentially damped/undamped sinusoids in noise," *IEEE Trans. Acoust., Speech, Signal Process.*, vol. 38, no. 5, pp. 814–824, 1990.

[24] Y. Hua, "Estimating two-dimensional frequencies by matrix enhancement and matrix pencil," *IEEE Trans. Signal Process.*, vol. 40, no. 9, pp. 2267–2280, 1992.

[25] E. J. Candès and T. Tao, "The Dantzig selector: Statistical estimation when p is much larger than n," *The Annals of Statistics*, vol. 35, no. 6, pp. 2313–2351, 2007.

[26] J. Li and P. Stoica, "MIMO radar with colocated antennas," *IEEE Signal Process. Mag.*, vol. 24, no. 5, pp. 106–114, 2007.

[27] ——, *MIMO Radar Signal Processing*. Hoboken, NJ, Wiley, 2009.

[28] T. J. Abatzoglou and W. Zhou, "Methods and systems for processing radar signals," US Patent App. 17/375,994, Issued on August 29, 2023.

[29] A. Ganis and *et al.*, "A portable 3-D imaging FMCW MIMO radar demonstrator with a 24x24 antenna array for medium-range applications," *IEEE Trans. Geosci. Remote Sens.*, vol. 56, no. 1, pp. 298–312, 2018.